Polarizability measurements of the 8s^{2}S_{1/2} and 9s^{2}S_{1/2} states of atomic cesium

H. Weaver and A. Kortyna

Phys. Rev. A **86**, 042511 — Published 19 October 2012

DOI: 10.1103/PhysRevA.86.042511

Polarizability measurements of the $8s\,^2S_{1/2}$ and $9s\,^2S_{1/2}$ states of atomic cesium

H. Weaver and A. Kortyna

Department of Physics, Lafayette College,

Easton, Pennsylvania 18042 U.S.A.

Abstract

We report hyperfine-resolved scalar polarizabilities for cesium's $8s\,^2S_{1/2}$ and $9s\,^2S_{1/2}$ states using resonant two-photon spectroscopy in both an effusive beam and a vapor cell. Electric-field strengths are measured *in situ*, and the frequency scale is directly referenced to the ground-state hyperfine splitting of atomic rubidium. The measured $8s\,^2S_{1/2}$ scalar polarizability is $38370 \pm 380\,a_0^3$ which agrees well with previously reported theoretical and experimental values. The measured $9s\,^2S_{1/2}$ scalar polarizability is $150700 \pm 1500\,a_0^3$ which agrees within two sigma with theory, but we are unaware of previous measurements. We verify that the $8s\,^2S_{1/2}$ state polarizability is independent of the hyperfine level, placing an upper limit of $200 \pm 260\,a_0^3$ on the differential polarizability — this agrees with previous observations. We also measure a null differential polarizability between the hyperfine levels for the $9s\,^2S_{1/2}$ of $490 \pm 450\,a_0^3$.

PACS numbers: 32.10.Dk,32.60.+i

I. INTRODUCTION

The accurate determination of atomic polarizabilities is motivated by many important applications. Examples include predicting transition rates, estimating cold and long-range molecular interactions, and optimizing optical cooling and trapping schemes,[1] as well as determining electric-field strengths in plasmas [2]. In particular, the present work is motivated by the ability of polarizabilities to provide benchmarking data for atomic-structure calculations. Atomic structure calculations are essential for interpreting atomic-physics measurements of parity-nonconserving interactions [3] where gauging computational reliability is critical for analyzing experimental results [4]. Atomic-structure calculations are also important for estimating blackbody radiation shifts which appears to be a significant limitation to the precision of next-generation optical frequency standards.[5] The ability to generate accurate polarizabilities is essential for computing precise blackbody radiation shifts.

Significant effort has been expended on determining the $ns\,^2S_{1/2}$ polarizabilities of atomic cesium. The scalar polarizabilities of the $6s\,^2S_{1/2}$ [6], the $7s\,^2S_{1/2}$ [7], and the $8s\,^2S_{1/2}$ [8, 9] states have been measured to high precision, as have the $ns\,^2S_{1/2}$ states for $n = 10 - 13$ [10]. All of these measurements agree well with polarizability calculations [11, 12]. These theoretical studies also compute the $9s\,^2S_{1/2}$ polarizabilities, but to the best of our knowledge, measurements for this state have not been reported in the literature.

The primary objective of the current article is to report the $9s\,^2S_{1/2}$ scalar polarizability measurement of atomic cesium. We use resonant two-photon spectroscopy to observe the hyperfine-resolved Stark effect in an effusive beam. The frequency scale is directly referenced to the ground hyperfine transition of atomic rubidium using a phase-modulation technique and absorption spectroscopy in a cesium vapor cell. The electric field is measured *in situ* by comparing the $6s\,^2S_{1/2} \rightarrow 6p\,^2P_{1/2}$ Stark shift with previous high-precision measurements [13]. To verify the accuracy and reliability of our experimental arrangement, we also measure the $8s\,^2S_{1/2}$ scalar polarizability, which agrees well with previous measurements [8, 9] and calculations [11, 12].

Using second order perturbation theory, the Stark shift ΔW can be written in terms of the scalar polarizability α_0 as

$$\Delta W = -\frac{1}{2}\alpha_0\epsilon^2 \tag{1}$$

where ϵ is the applied electric field strength. For our resonant two-step excitation scheme,

we measure the effective Stark shift of the $6p\,^2P_{1/2} \rightarrow ns\,^2S_{1/2}$ transition ΔW_{ns},

$$\Delta W_{ns} = -\frac{1}{2}[\alpha_0(ns_{1/2}) - \alpha_0(6p_{1/2})]\epsilon^2 \tag{2}$$

where $n = 8$ and 9, $\alpha_0(ns_{1/2})$ is the scalar polarizability of the $ns\,^2S_{1/2}$ state, and $\alpha_0(6p_{1/2})$ is the scalar polarizability of the $6p\,^2P_{1/2}$ state. With the high precision Stark shift measurements for the $6s\,^2S_{1/2} \rightarrow 6p\,^2P_{1/2}$ transition [13] and the $6s\,^2S_{1/2}$ polarizability [6], we determine $\alpha_0(6p_{1/2})$ and solve Eq. 2 for $\alpha_0(ns_{1/2})$.

The scalar polarizability term shifts each state of a hyperfine manifold by equal amounts. There is also a tensor polarizability term that mixes the various magnetic sublevels of the hyperfine manifold.[14] This leads to differential Stark shifts and splittings of the magnetic sublevels. The tensor polarizability term, however, has been omitted from Eqs. 1 and 2 because it is predicted to be negligible for $ns\,^2S_{1/2}$ states [15]. As expected, we observe no evidence of mixing or splitting, and conclude that the magnitude of the tensor term is well below our detection sensitivity.

There is also a hyperfine interaction that produces differential polarizabilities. This differential polarizability has been computed for the ground state of atomic cesium as being a factor of 10^{-6} that of the respective scalar polarizabilities.[16] Because of its small relative magnitude, its effect is assumed to be zero for both the ground and excited states when interpretating parity-nonconserving measurements of the $6s_{1/2} \rightarrow 7s_{1/2}$ transition [3]. A non-zero hyperfine interaction would, therefore, impact the interpretation of these results. The possibility that the hyperfine dependence of the polarizabilities is significantly larger than previously thought has been raised by Ref. [8], who measured a 1% effect for the $8s\,^2S_{1/2}$ state. However, Antypas and Elliott [9] subsequently set an upper limit on the $8s\,^2S_{1/2}$ differential hyperfine polarizability of 0.15%. We verify Antypas and Elliott's findings for the $8s\,^2S_{1/2}$ state, and place an upper limit for the $9s\,^2S_{1/2}$ of 0.3%.

II. EXPERIMENT

The hyperfine-resolved Stark shifts of the $8s\,^2S_{1/2}$ and $9s\,^2S_{1/2}$ states of atomic cesium are measured using an apparatus similar to that described in Ref. [17]. An abbreviated diagram of the apparatus appears in Fig. 1. Briefly, two single-mode external-cavity diode lasers probe the $6s\,^2S_{1/2}(F'' = 4) \rightarrow 6p\,^2P_{1/2}(F') \rightarrow \ ns\,^2S_{1/2}(F = 3 \text{ and } 4)$ two-photon transition

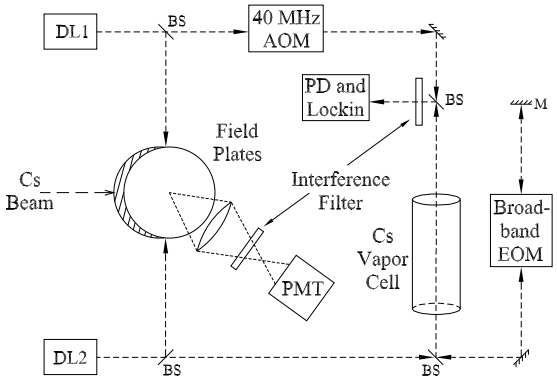

FIG. 1. Resonant two-photon apparatus for measuring Stark shifts of cesium's $8s\,^2S_{1/2}$ and $9s\,^2S_{1/2}$ states. The Stark shift is measured in an effusive beam by applying an electric field across parallel plates, and the frequency scale is calibrated by phase modulating the DL2 laser beam prior to passing through the vapor cell. Symbol key: 40MHz AOM — 40MHz acousto-optical modulator; Broadband EOM — 1-250MHz electro-optical modulator; BS — beam splitter; DL1 and DL2 — single-mode external-cavity diode lasers; PD and Lockin — photodiode and phase-sensitive lockin amplifier; PMT — photomultiplier tube.

simultaneously in a collimated effusive beam and in a vapor cell. One laser (DL1 in Fig. 1) is locked to the center of the $6s\,^2S_{1/2}(F''=4) \rightarrow 6p\,^2P_{1/2}(F')$ transition at 894.59 nm using a saturated-absorption spectrometer. The second laser (DL2) is stepped across the $6p\,^2P_{1/2}(F') \rightarrow ns\,^2S_{1/2}(F=3 \text{ or } 4)$ transition at 761.10 nm for $n=8$ and 635.63 nm for $n=9$. Figure 2 shows a schematic of the relevant energy levels and transitions. Laser beam intensities are held below $1.0\,\mathrm{mW/cm^2}$ to eliminate the power broadening of spectral features. The drift rate of DL2 is on the order 25 MHz/hour. To minimize the effect of this drift on measured frequency intervals, we collect data by scanning the DL2 frequency in both directions for each data collection run, and storing the two spectra separately. Any drift accumulated during one scan should, on average, be canceled by the subsequent scan in the opposite direction. In addition, our frequency calibration technique (see below) has been demonstrated to effectively cancels out the laser frequency drift [17].

Both laser beams are split and simultaneously counter-propagated through the effusive beam and the vapor cell. A dual fluorescence-absorption spectrum is thus generated:

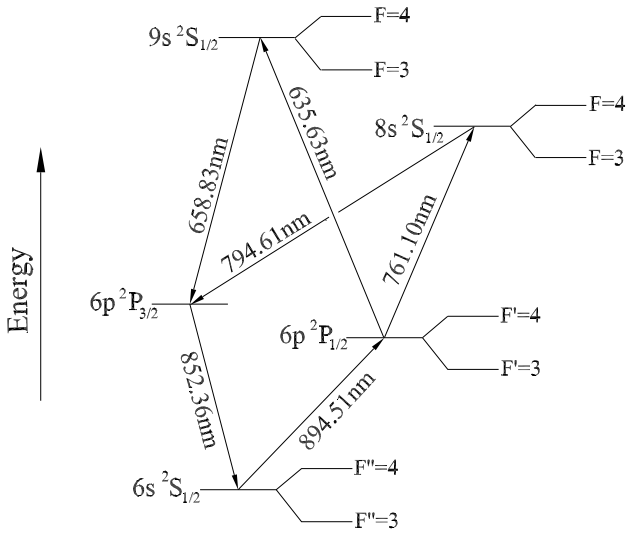

FIG. 2. Relevant energy levels (not to scale) and the laser excitation/detection scheme. Two single-mode diode lasers excite the $6s\,^2S_{1/2}(F''=4) \rightarrow 6p\,^2P_{1/2}(F') \rightarrow ns\,^2S_{1/2}(F)$ double-resonant transition in cesium. Absorption (at 761.10 nm for $n = 8$ and 635.83 nm for $n = 9$) is monitored in the vapor cell, and fluorescence (at 794.61nm for the $n = 8$ state and 658.83nm for $n = 9$) is monitored from the effusive beam.

the Stark shift is measured in the effusive beam through laser-induced-fluorescence (LIF) spectroscopy, and the frequency scale is calibrated in the vapor cell through absorption spectroscopy and phase-sensitive signal detection. To implement phase-sensitive detection, the DL1 laser beam is amplitude modulated at about 17 kHz with a 40 MHz acusto-optic modulator (AOM). The DL2 beam counter-propagates through the absorption cell and is detected by a photo-diode and lock-in amplifier. As DL2 is stepped across the $6p\,^2P_{1/2}(F') \rightarrow ns\,^2S_{1/2}(F)$ transition, the output of the lock-in amplifier is recorded by an analog-to-digital converter and stored as a function of laser detuning.

The vapor cell is held in a field-free region and a modulation technique provides frequency calibration. This calibration technique was introduced in Ref. [18]. It was further developed and described in detail in Ref. [17]. The DL2 beam double passes an electro-optic modulator (EOM) driven at either 100 MHz (for $8s\,^2S_{1/2}$ measurements) or 120 MHz (for $9s\,^2S_{1/2}$ measurements). These frequencies are directly referenced to a 10 MHz ^{87}Rb frequency standard that provides both short-term stability and long-term accuracy to better than 5 parts in 10^9. The double-pass configuration allows the EOM to impose second-order, and sometimes even

third-order sidebands onto the laser frequency. When the modulated laser is stepped across a spectroscopic feature, that feature is observed once for each sideband. A frequency-scale-calibration function is obtained by fitting a second-order polynomial to the positions of the five to seven modulation-induced features. The multiple sidebands also provide a measure of the nonlinearity of the laser frequency scan.

To evaluate the precision of our calibration function, we fit third-order polynomials to a random sampling of spectra. The cubic terms are found to be a factor of 10^8 smaller than the linear terms and 10^3 smaller than the quadratic terms. In a large majority of the cases, the cubic terms are not statistically significant, and at most, they are only marginally statistically significant. We estimate the uncertainty created by ignoring the cubic term to be no larger than 1% of the overall uncertainty budget.

The effusive beam apparatus and the technique for driving and detecting a two-photon transition in the effusive beam is detailed in Refs. [19, 20]. The effusive beam source is held at 200°C, producing a cesium backing pressure of 0.1 mbar. The beam is collimated by a pair of apertures to a divergence of 4.2 mrad such that the transverse Doppler broadening is 4.7 MHz for the $8s\,^2S_{1/2}$ state and 5.6 MHz for the $9s\,^2S_{1/2}$ state. The cesium flux at the interaction region is about 10^{10} atom/s. The counter-propagating laser beams intersect the effusive beam a right angles. Fluorescence from the $ns\,^2S_{1/2} \rightarrow 6p\,^2P_{3/2} \rightarrow 6s\,^2S_{1/2}$ cascade is collected by a lens and detected in a photomultiplier tube (PMT). Interference filters pass fluorescence from the $ns_{1/2} \rightarrow 6p_{3/2}$ transition (794.61nm for the $n = 8$ state and 658.83nm for $n = 9$). The PMT count rate is accumulated by a counter-timer board and stored alongside the absorption signal. Possible systematic errors arising from the residual magnetic field are minimized by linearly polarizing both laser beams (parallel to the effusive-beam axis) to suppress $\Delta m \neq 0$ transitions [21]. We also reduce the residual magnetic field in the Stark-shift region below 50 mGauss with high-permeability shielding.

III. ELECTRIC FIELD MEASUREMENT AND DETERMINATION OF α_0

Stark shifts are induced in the effusive beam by applying a uniform electric field across two parallel copper plates (90mm in diameter, ground to a flatness of ± 0.05 mm and separated by 6.35 ± 0.16 mm). These plates are centered on the intersection of the effusive beam and the counter-propagating laser beams. An electric potential of up to 4.5 kV is applied across

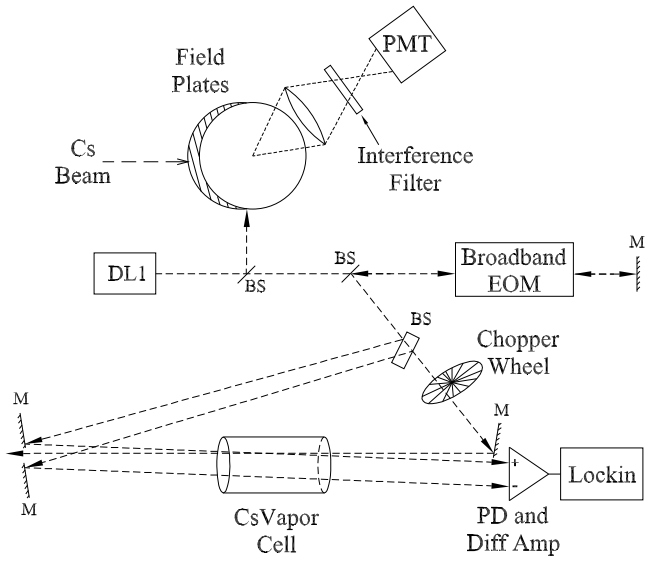

FIG. 3. Effusive-beam/saturated-absorption setup for calibrating the electric-field strength. The $6s\,^2S_{1/2} \rightarrow 6p\,^2P_{1/2}$ Stark shift is measured in the effusive beam, and the frequency scale is calibrated by phase modulating the laser prior to entering the saturated-absorption spectrometer. Symbol key: Broadband EOM — 1-250MHz electro-optical modulator; BS — beam splitter; DL1 — single-mode external-cavity diode lasers; M — mirror; PD and Diff Amp — photodiodes and differential amplifier: PMT — photomultiplier tube.

these plates with the potentials on the top and bottom plates applied symmetrically about ground. Each electric potential is monitored using a precision voltmeter (certified accuracy of eight parts in 10^5) and precision 2000:1 voltage dividers with a measured accuracy of one part in 10^4.

Instead of making absolute determinations of the plate separation and the potential differences across the plates, we relax the electro-mechanical demands of measuring the electric field by using an *in situ* atomic-physics-based method. This method essentially converts the electric field measurement into a frequency-difference determination. The experimental setup for electric-field calibration is illustrated in Fig. 3. We put significant effort into making the field plates as parallel as possible, but only estimate their absolute separation. To accurately obtain the electric-field strength at any applied potential difference, we measure the Stark shift for the $6s\,^2S_{1/2} \rightarrow 6p\,^2P_{1/2}$ transition and compare this to high-precision measurements cited in the literature [13]. We use only DL1 for electric-field calibration, and step

its frequency across the $6s\,^2S_{1/2}(F=4) \rightarrow 6p\,^2P_{1/2}(F=3 \text{ or } 4)$ transition in both directions. Similar to our method of measuring the $ns\,^2S_{1/2}$ polarizabilities described in Sec. II, the laser beam passes simultaneously through the effusive beam and the saturated-absorption spectrometer. The Stark shift is measured in the effusive beam, and the frequency scale is calibrated by imposing modulation sidebands onto the laser frequency prior to the beam entering the saturated-absorption spectrometer. The modulation frequency is set at 35 MHz for this measurement.

To obtain the electric-field-calibration factor, we write the *true* Stark shift of the $6s\,^2S_{1/2} \rightarrow 6p\,^2P_{1/2}$ transition, ΔW_{6p}, as

$$\Delta W_{6p} = -\frac{1}{2}[\alpha_0(6p_{1/2}) - \alpha_0(6s_{1/2})]\epsilon^2. \tag{3}$$

We then assume that the measured Stark shift, W_{6p}^{meas}, can be expressed as

$$\Delta W_{6p}^{meas} = -\frac{1}{2}[\alpha_0(6p_{1/2}) - \alpha_0(6s_{1/2})](\xi\epsilon_{est})^2 \tag{4}$$

where ϵ_{est} is the electric field estimated from our measured electric potential and plate separation, and ξ is the correction factor relating the true electric field, ϵ, to the estimated electric field, ϵ_{est}. The correction factor squared, ξ^2, is found by dividing Eq. 4 by Eq. 3. In practice, we find ξ^2 by plotting W_{6p}^{meas} as a function of ϵ_{est}^2, and compute the least-squares slope, $\partial(\Delta W_{6p}^{meas})/\partial\epsilon_{est}^2$. Using Eq. 4, we express this slope as

$$\frac{\partial(\Delta W_{6p}^{meas})}{\partial\epsilon_{est}^2} = -\frac{1}{2}[\alpha_0(6p_{1/2}) - \alpha_0(6s_{1/2})]\xi^2 \tag{5}$$

where the effective polarizability, $\alpha_0(6p_{1/2}) - \alpha_0(6s_{1/2})$, is provided by Ref. [13]. When determining the slope, the higher-order terms are always statistically insignificant. To check for consistency, we carry out this proceedure for both $6p\,^2P_{1/2}$ hyperfine states ($F' = 3$ and 4). As expected, no significant difference is observed. For most of the data presented in this report, $\xi^2 = 0.9071 \pm 0.0088$.

Once the electric-field strength is calibrated, the $ns\,^2S_{1/2}$ polarizability $\alpha_0(ns_{1/2})$ can be determined from Eq. 2 by using $\epsilon^2 = (\xi\epsilon_{est})^2$. If $\partial(\Delta W_{ns}^{meas})/\partial\epsilon_{est}^2$ is the least-squares slope when plotting ΔW_{ns}^{meas} against ϵ_{est}^2, Eq. 2 can be solved for the sought after polarizability

$$\alpha_0(ns) = \alpha_0(6p_{1/2}) - \frac{2}{\xi^2}\frac{\partial(\Delta W_{ns}^{meas})}{\partial\epsilon_{est}^2}. \tag{6}$$

This electric-field-calibration method improves our polarizability resolution by a factor of five over our previous electro-mechanical method [17].

IV. RESULTS AND DATA ANALYSIS

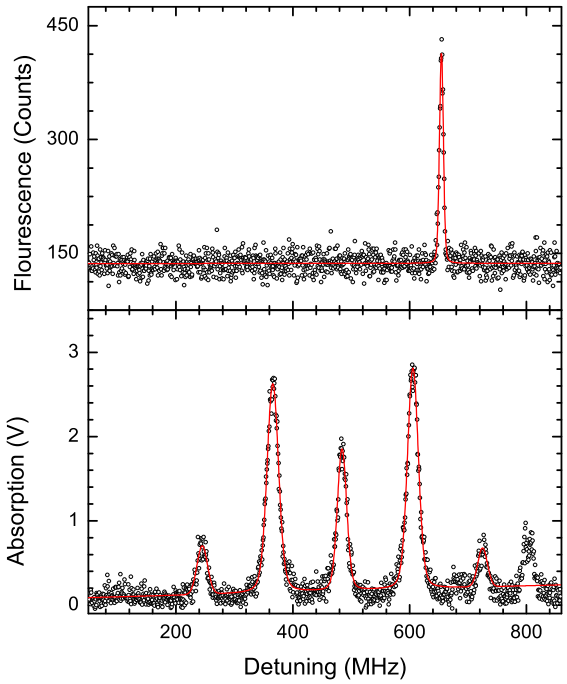

FIG. 4. (Color online) Dual two-photon fluorescence-absorption spectrum of the Cs $6s\,^2S_{1/2}(F''=4) \rightarrow 6p\,^2P_{1/2}(F'=3) \rightarrow\ 9s\,^2S_{1/2}(F=4)$) transition. The open circles are data and the solid lines are fitted Voigt profiles. Upper panel: laser-induced-fluorescence signal from the effusive beam at an electric field strength of 3.19 kV/cm. Lower panel: absorption signal from the field-free vapor cell. The Stark shift is determined from the difference between the fluorescence peak centroid and the central absorption peak centroid. The absorption spectrum is used for frequency-calibration by phase modulating the scanned laser at 120 MHz. The first- and second-order modulation sidebands are clearly visible in this spectrum. Also visible (at about 805 MHz) is a modulation sideband from the $9s\,^2S_{1/2}(F=3)$ state which is not used in the analysis.

Figure 4 shows a typical dual fluorescence-absorption specrtrum used for determining Stark shift, in this case for the $9s\,^2S_{1/2}(F=4)$ state. Both plots show the resonant two-photon signal from the $6s\,^2S_{1/2}(F''=4) \rightarrow 6p\,^2{}_{1/2}(F'=3) \rightarrow\ 9s\,^2S_{1/2}(F=4)$ transitions of cesium with the DL2 frequency stepped across 1200 points. The upper panel is the LIF signal

from the effusive beam as a function of the DL2 detuning frequency collected at 3.19 kV/cm. The lower panel is the absorption spectrum collected in the field-free vapor cell with 120 MHz modulation sidebands imposed on DL2. Also included in both panels are Voigt profiles fitted to each spectral line using a Levenburg-Marquardt residual minimization algorithm.

For the fluorescence signal from the effusive beam, peak widths (full width half maximum) are found to be 8 ± 1 MHz and the centroids are determined within 150 kHz. The peak widths show no dependence on the applied field, indicating that the magnitude of the tensor polarizability is below our experimental sensitivity: splitting of the magnetic sublevels would first be observed as broadening of the peak widths. Given the natural linewidth of 4.6 MHz for the $6p\,^2P_{1/2}$ state [22] and 0.92 MHz for the $9s\,^2S_{1/2}$ state [23], the two-photon linewidth should be 1.7 MHz [24]. Combining this linewidth with the effusive beam's transverse Doppler width and the 1 MHz laser bandwidth in quadrature yields an expected linewidth of about 6 MHz, which is in reasonable agreement with the observed widths.

For the cell, peak widths are 20 ± 2 MHz and the centroids are determined within 300 kHz. The cell linewidth likely reflects residual Doppler broadening due to imperfect counter-propagation of the laser beams.

To quantify the Stark shift, we apply a potential difference across the field plates and collect the dual fluorescence-absorption spectrum as illustrated in Fig. 4. After calibrating the frequency scale (see in Sec. II), we determine the frequency difference between the Stark-shifted fluorescence peak and the central absorption peak from the field-free vapor cell. We collect a number of dual spectra at one particular electric field, and then step the electric field evenly across the 0 — 7.1 kV/cm range. The Stark-shift results are summarized as linearized plots in Fig. 5 for the $8s\,^2S_{1/2}(F=3)$ state and in Fig. 6 for the $9s\,^2S_{1/2}(F=3)$ state. Data for the $8s\,^2S_{1/2}(F=4)$ and $9s\,^2S_{1/2}(F=4)$ states are analyzed in the same way and included in our results.

Polarizabilities are computed using Eq. 6 and summarized in Table I. The uncertainties are a quadrature combination of the error budget given in Table II. The reference-frequency uncertainty $\delta\nu/\nu$ is due to long-term drifts and short term stability of the 10 MHz rubidium frequency standard. The third-order fit uncertainty ($\delta\nu_3/\nu_3$) is estimated by examining the magnitude of the cubic term of the frequency calibration function relative to the linear and quadratic terms. In practice, however, only second-order fits are used for frequency calibration. The electric-field calibration uncertainty is the standard error generated by the

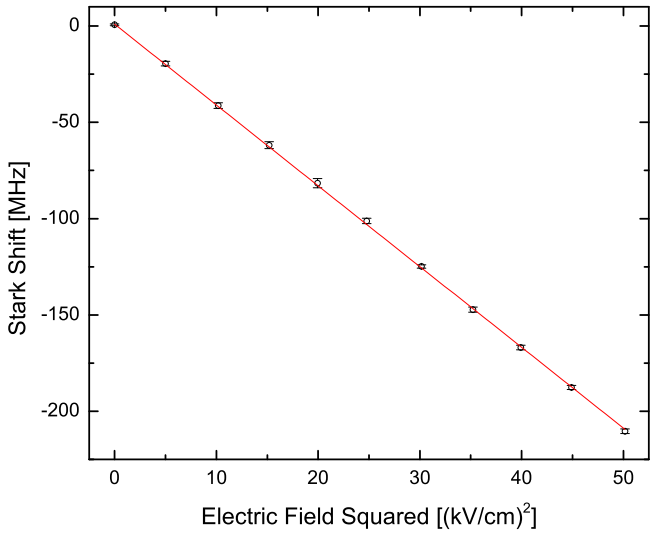

FIG. 5. (Color online) Net Stark shift of the $8s_{1/2}(F=3)$ state. A linear least squares fit gives a slope of $-4.196 \pm 0.012\,\mathrm{MHz}/(\mathrm{kV/cm})^2$ or $-16863 \pm 48\,a_0^3$. Error bars indicate three sigma.

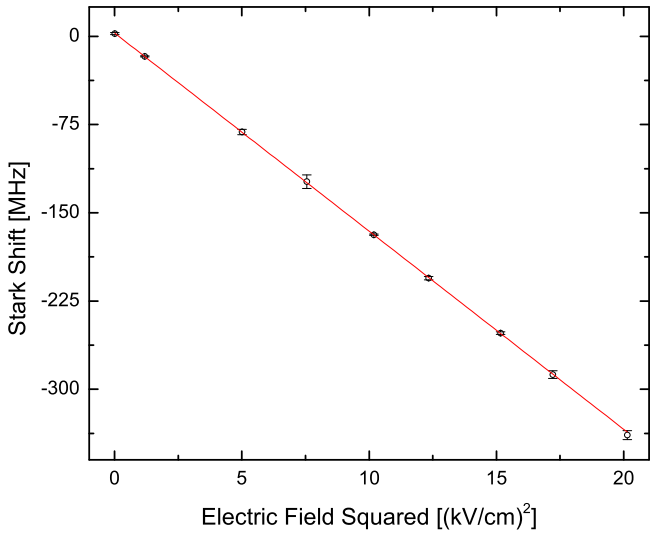

FIG. 6. (Color online) Net Stark shift of the $9s_{1/2}(F=3)$ state. A linear least squares fit gives a slope of $-16.837 \pm 0.018\,\mathrm{MHz}/(\mathrm{kV/cm})^2$ or $-67664 \pm 72\,a_0^3$. Error bars indicate three sigma.

TABLE I. Scalar polarizability of the $8s\,^2S_{1/2}$ and $9s\,^2S_{1/2}$ states of atomic cesium in units of a_0^3. Our experimental uncertainties are the quadrature combination of statistical and systematic uncertainties. Also listed are experimental values from the literature for the $8s\,^2S_{1/2}$ state (Exp.) and two calculations for both states: a Coulomb approximation method (CA) and a relativistic all-order closed coupling method (RAOCC).

	$8s\,^2S_{1/2}$	$9s\,^2S_{1/2}$
Present	38370 ± 380	150700 ± 1500
CA [11]	37900	153000
RAOCC [1, 12]	38270 ± 280	153700 ± 1000
Exp. [8]	38260 ± 290	—
Exp. [9]	38110 ± 50	—

electric field calibration procedure.

For the $8s\,^2S_{1/2}$ polarizability, our results are in very good agreement with the literature. Our measurements are within one sigma of two previous measurements using multiphoton non-resonant excitation [8, 9]. Our measurements also agree with two previous theoretical values [11, 12]. For the $9s\,^2S_{1/2}$ polarizability, we are not aware of previously reported measurements, but our results agree with both the Coulomb Approximation [11] and the relativistic all-order closed coupling method [12]. However, the difference is less than two sigma of the combined experimental-theoretical uncertainty for the more accurate relativistic all-order closed coupling method. Our measurements show good reproducibility. On the first day of data collection for the $9s\,^2S_{1/2}$ state, we measured a scalar polarizability of $150800 \pm 1500\,a_0^3$. Several months later, we recalibrated the electric field and measured a polarizability of $150600 \pm 1500\,a_0^3$. The value given in Table I is a combination of these two measurements where the uncertainty is dominated by the systematics of the electric field.

We also measured a null value for the hyperfine dependence of the polarizability for both states. For the $8s\,^2S_{1/2}$ state, the differential polarizability is $\Delta\alpha_{8s} = 200 \pm 260\,a_0^3$. For the $9s\,^2S_{1/2}$ state, the differential polarizability is $\Delta\alpha_{9s} = 490 \pm 450\,a_0^3$. These results are in agreement with previous observations for the $8s\,^2S_{1/2}$ state [9], and comply with expectations [16].

TABLE II. Uncertainty budget: uncertainties are given as relative values.

Reference frequency ($\delta\nu/\nu$):	2×10^{-10}
Third-order fit ($\delta\nu_3/\nu_3$):	1×10^{-4}
Electric field calibration ($2\ \delta\epsilon/\epsilon$):	9.7×10^{-3}
Statistical ($8s\,^2S_{1/2}$):	1.3×10^{-3}
Statistical ($9s\,^2S_{1/2}$):	7.2×10^{-4}

V. CONCLUSION

We measure the scalar polarizabilities of the $8s\,^2S_{1/2}$ and $9s\,^2S_{1/2}$ states of atomic cesium using two-photon resonant spectroscopy. Stark shifts are observed through laser-induced fluorescence from an effusive beam, and the frequency scale is calibrated concurrently using a phase-modulated absorption signal in a vapor cell. The electric-field strength is determined *in situ* by measuring the Stark shift of the $6p\,^2P_{1/2}$ polarizability. Our measurements of $38370 \pm 380\,a_0^3$ for the $8s\,^2S_{1/2}$ and $150700 \pm 1500\,a_0^3$ for the $9s\,^2S_{1/2}$ states of atomic cesium are in good agreement with previous measurements for the $8s\,^2S_{1/2}$ state [8, 9] and with theory for both states [11, 12]. We also place upper limits on the hyperfine dependence of the polarizabilities: $200 \pm 260\,a_0^3$ for the $8s\,^2S_{1/2}$ state and $490 \pm 450\,a_0^3$ for the $9s\,^2S_{1/2}$ state.

ACKNOWLEDGMENTS

This work was supported by the National Science Foundation under Grant No. PHYS-0653107. We thank Marianna Safronova, University of Delaware, for assistance with evaluating the theory associated with these measurements. We express our sincere gratitude to the late Richard Mertz, former Physics Department Technician, for his assistance in fabricating the experimental apparatus.

[1] J. Mitroy, M. S. Safronova, and C. W. Clark, J. Phys. B **43**, 202001 (2010).

[2] J. E. Lawler and D. A. Doughty, Adv. At. Mol. Opt. Phys. **34**, 171 (1995).

[3] C. Wood, S. Bennett, D. Cho, B. Masterson, J. Roberts, C. Tanner, and C. Wieman, Science **275**, 1759 (1997).

[4] S. C. Bennett and C. E. Wieman, Phys. Rev. Lett. **82**, 2484 (1999).

[5] M. S. Safronova, D. Jiang, B. Arora, C. W. Clark, M. G. Kozlov, U. I. Safronova, and W. R. Johnson, IEEE Trans. Ultrason. Ferroelectrics and Frequency Control **57**, 94 (2010).

[6] J. M. Amini and H. Gould, Phys. Rev. Lett. **91**, 153001 (2003).

[7] S. C. Bennett, J. L. Roberts, and C. E. Wieman, Phys. Rev. A **59**, R16 (1999).

[8] M. Gunawardena, D. S. Elliott, M. S. Safronova, and U. Safronova, Phys. Rev. A **75**, 022507 (2007).

[9] D. Antypas and D. S. Elliott, Phys. Rev. A **83**, 062511 (2011).

[10] W. A. van Wijngaarden, E. A. Hessels, J. Li, and N. E. Rothery, Phys. Rev. A **49**, R2220 (1994).

[11] W. A. van Wijngaarden and J. Li, J. Quant. Spect. Rad. Transf. **52**, 555 (1994).

[12] E. Iskrenova-Tchoukova, M. S. Safronova, and U. I. Safronova, J. Comput. Meth. Sci. Eng. **7**, 521 (2007).

[13] L. R. Hunter, D. Krause, K. E. Miller, D. J. Berkeland, and M. B. Boshier, Opt. Comm. **94**, 210 (1992).

[14] R. Schmeider, Am. J. Phys. **40**, 297 (1972).

[15] J. R. P. Angel and P. G. H. Sandars, Proc. Royal Soc. London A **305**, 125 (1968).

[16] J. D. Feichtner, M. E. Hoover, and M. Mizushima, Phys. Rev. **137**, A702 (1965).

[17] A. Kortyna, C. Tinsman, J. Grab, M. S. Safronova, and U. I. Safronova, Phys. Rev. A **83**, 042511 (2011).

[18] A. Kortyna, N. A. Masluk, and T. Bragdon, Phys. Rev. A **74**, 022503 (2006).

[19] A. Kortyna, V. Fiore, and J. Farrar, Phys. Rev. A **77**, 062505 (2008).

[20] A. Kortyna, V. Fiore, and J. Farrar, Phys. Rev. A **78**, 019901(E) (2008).

[21] Note1, magnetic sublevels with the same quantum numbers tend to have similar Zeeman shifts.

[22] C. Amiot, O. Dulieu, R. F. Gutterres, and F. Masnou-Seeuws, Phys. Rev. A **66**, 052506 (2002).

[23] J. Marek, Phys. Lett. **60A**, 190 (1977).

[24] J. E. Bjorkholm, , and P. R. Liao, Phys. Rev. A **14**, 751 (1976).